Geophysical Journal International

*Geophys. J. Int.* (2023) **234,** 870–878
Advance Access publication 2023 March 11
GJI Seismology

https://doi.org/10.1093/gji/ggad109

# Simulating H/V spectral ratios (HVSR) of ambient vibrations: a comparison among numerical models

D. Albarello,[1,2] M. Herak,[3] E. Lunedei,[1] E. Paolucci[1] and A. Tanzini[1]

[1]*Department of Physics, Earth and Environmental Sciences, University of Siena, Siena* 53100*, Italy. E-mail: dario.albarello@unisi.it*
[2]*Consiglio Nazionale delle Ricerche, Istituto di Geologia Ambientale e Geoingegneria,* 00185 *Roma, Italy*
[3]*Department of Geophysics, Faculty of Science, University of Zagreb,* 10000 *Zagreb, Croatia*

Accepted 2023 March 6. Received 2023 February 11; in original form 2022 October 24

## SUMMARY

The use of H/V spectral ratios (HVSR) of ambient vibrations to constrain the local seismo-stratigraphical configuration relies on numerical forward models able to connect observations with subsoil seismic properties. Several models were proposed to this purpose in the last decades, which are based on different assumptions about the nature of the ambient vibration wavefield. Performances of nine numerical tools implementing these models have been checked by considering 1600 realistic 1-D subsoil configurations mostly relative to A, B and C Eurocode8 soil classes. Resultant HVSR curves predicted by the models are quite similar both in their general shape and in predicting the resonant soil frequencies, possibly because all of them share the same basic representation of the subsoil as a 1-D stack of flat uniform viscoelastic layers. The common sensitivity to transmission/reflection matrices resulting from that representation explains the well-known correspondence of HVSR maxima to 1-D resonance frequency estimates, regardless of the physical assumptions (about source distribution, radiation pattern, dominating seismic phases, etc.) behind the computational model adopted for simulating HVSR curves. On the other hand, the computational models here considered provide quite different amplitudes for HVSR values corresponding to the resonance frequencies. However, since experimental HVSR amplitudes at the same site are affected by an inherent variability (e.g. due to the possible lack of ergodicity of the ambient vibration stochastic wavefield, non-ideal experimental settings, etc.) and uncertainty about the local seismo-stratigraphical profile (attenuation, 2-D/3-D effects, etc.) observations cannot be used for general scoring of the considered computational models on empirical basis. In this situation, the 'optimal' numerical tool to be considered for the forward HVSR modelling must be defined case by case.

**Key words:** Numerical modelling; Computational seismology; Seismic noise; Site effects.

## 1 INTRODUCTION

The ambient vibration wavefield is the object of seismological research since the XIX century (Ferrari *et al.* 2000). Starting from the second half of the last century, a lot of effort has been made to extract information about the seismic properties of the subsoil from ambient vibrations by the analysis of seismometric data obtained from seismic arrays (e.g. Okada 2003) and single station (e.g. Bard *et al.* 2005) experimental settings. The first configuration aims at the characterization of surface waves propagation pattern by determining modal or effective dispersion curves relative to Rayleigh and Love wave components of the ambient vibration wavefield. In the single station configuration, ratios of average spectral amplitudes of horizontal and vertical components of ambient vibrations measured at the Earth surface as a function of frequency (hereafter 'HVSR curve' where HVSR stands for Horizontal to Vertical Spectral Ratios) are considered to identify seismic resonance phenomena of the shallow subsoil (Molnar *et al.* 2022).

The joint inversion of surface wave dispersion and HVSR curves aims at constraining the local *Vs* profile in engineering applications (e.g. Foti *et al.* 2011). To this purpose, suitable numerical models are required for the forward modelling of experimental curves starting from a subsoil configuration used as a guess. While forward modelling of surface waves dispersion curves is relatively well established at least for 1-D subsoil configurations (e.g. Schwab & Knopoff 1972; Foti *et al.* 2015), more complex and controversial appears the situation regarding the HVSR curve. Spectral amplitude of ambient vibrations is the result of a complex combination

of all seismic phases whose respective contribution is expected to depend on the structure and distribution of the relevant sources and the subsoil configuration.

To manage this complex situation, several approaches have been proposed by adopting more or less restrictive assumptions concerning the ambient vibration wavefield (Lunedei & Malischewsky 2015). The simplest approach was proposed by Herak (2008) by assuming that HVSR curve relative to any 1-D subsoil configuration only depends on the soil response (amplification spectra) due to vertically propagating body waves. Many other approaches assume that surface waves play a major role in ambient vibration. In the simplest cases, HVSR is considered as an expression of Rayleigh waves ellipticity (Malischewsky & Scherbaum 2004). A more complex approach includes in the modelling Rayleigh and Love waves in their fundamental and higher modes as generated by a uniform distribution of random uncorrelated point sources (Lanchet & Bard 1994, 1995; Arai & Tokimatsu 2004; Lunedei & Albarello 2009). More recently full wavefield models have been proposed by considering a distribution of uncorrelated or correlated random point-like (Lunedei & Albarello 2010, 2015) or extended (Lunedei & Albarello 2021) surface sources. A different approach releases the assumption of surface sources by considering a diffuse field generated by sources distributed in the subsurface halfspace to simulate scattering of seismic waves (Sanchez-Sesma *et al.* 2011). The release of restrictive assumptions (e.g. concerning the seismic phases considered in the computational model), aiming at providing a more comprehensive representation of ambient vibrations, increases at the same time the numerical challenges concerning relevant computations. Those numerical difficulties occur because such models generally imply integration of rapidly oscillating functions in the frequency-wavenumber domain in the presence of poles which require specific and numerically troublesome procedures to prevent numerical instabilities. It is worth to note that, beyond relative differences, all the above models consider the subsoil as a stack of flat uniform elastic or viscoelastic layers, each characterized in terms of thickness, body wave velocities, density, and possibly, damping.

All these approaches are claimed to provide effective numerical tools for the forward modelling of HVSR curves and are currently used in engineering applications. However, due to strong differences in underlying assumptions, one may ask at what extent they are mutually compatible and provide feasible results when compared with observations. The empirical scoring of these models is not an easy task. To this purpose, in fact, one should compare observed HVSR curves with the theoretical ones inferred by considering available borehole data. However, the assumption that ambient vibration random field can be considered as fully ergodic is partially in contrast with observations suggesting that the physical structure of the ambient vibration wavefield (mostly, but not only, beyond 1 Hz) may change in the medium term (days, months) due to variations in the source nature and distribution (e.g. Marzorati & Bindi 2006; Paolucci *et al.* 2015). These variations cannot be averaged out when ambient vibrations are monitored for a relatively short time (from tens of minutes to hours) as is the common practice.

Moreover, the detailed knowledge of seismic properties of the subsoil are generally incomplete due to depth limitation of borehole data and inherent uncertainty concerning important parameters (e.g. damping profile). Finally, the empirical determination of experimental HVSR curves relies on several numerical manipulations (filtering, spectral smoothing, window selection, averaging horizontal components, etc.) and experimental settings (instrumental response to weak signal, soil/sensor coupling, environmental conditions, etc.) which makes the definition of the 'true' experimental HVSR curve to some extent controversial.

A different and less ambitious approach is considered in this paper, aiming at evaluating to what extent the proposed modelling procedures provide different outcomes when applied to the same subsoil configuration. If these outcomes turn out to be significantly different, one may infer that the empirical results might potentially discriminate the more effective ones. To this purpose, nine computational models proposed in the current literature are applied to simulate HVSR curves relative to a large set of realistic seismo-stratigraphical configurations representative of different geological domains (foredeep basins, mountain belts, volcanic environments, etc.). Then, the resulting HVSR curves are compared to evaluate possible systematic differences among outcomes of the considered computational models.

## 2 REPRESENTATIVE 1D SEISMO-STRATIGRAPHICAL CONFIGURATIONS

The soil profiles considered here result from numerical simulations using the litho-stratigraphic configurations observed along the geotraverse crossing the Apenninic orogenic belt, which represents a typical chain-foredeep-foreland system (Pieri *et al.* 2004; Finetti 2005). The seismic parameters have been retrieved by consulting a large database of subsoil data provided by seismic microzonation studies carried out in Southern Italy and managed by local authorities under the coordination of the Italian Centre for Seismic Microzonation and Applications (Moscatelli *et al.* 2020). The approach considered to define representative seismo-stratigraphical configurations is described in detail by Peruzzi *et al.* (2016), Paolucci *et al.* (2020, 2023) and is briefly outlined in the following.

Based on available information, a set of seismo-stratigraphical configurations is identified in the form of a stack of engineering geological units (Amanti *et al.* 2020) each characterized by a range of variation of respective depths and shear wave velocities (*Vs*). By considering these ranges, 200 profiles for each configuration were randomly generated using the approach implemented in the code STRATA (Kottke & Rathje 2008). To avoid unrealistic configurations generated by randomly changing *Vs* values of subsequent layers, an inter-layer correlation has been assumed which increases with depth by following the 'Geomatrix' configuration described by Toro (1995). A constant Poisson ratio (0.4) has been assumed for all the layers. Damping was assumed constant and very low (0.01) to simulate nearly elastic behaviour, because the considered computational models manage damping in different ways or simply discard it. Density has been estimated by following Brocher (2005). The resulting 1600 profiles reach a maximum depth of 170 m with a minimum *Vs* value of 160 m s$^{-1}$. In terms of EC8 soil classification (EN 1998-1), 122 profiles are of class A (Vs30 $>$ 800 m s$^{-1}$ corresponding to the engineering bedrock), 1198 of class B (Vs30 in the range 360–800 m s$^{-1}$ and depth of the engineering bedrock above several tens of m), 262 of class C (Vs30 in the range 180–360 m s$^{-1}$ and depth of the engineering bedrock above several tens of m), and 18 of Class E (Vs30 lower than 360 m s$^{-1}$ and depth of the engineering bedrock $<$20 m). No class D (Vs30 $<$180 m s$^{-1}$, depth of the engineering bedrock above several tens of m) profiles were generated by the randomization procedure. This distribution mimics the one relative to the *Vs* profiles in the Kik-Net database (Zhu *et al*. 2019; Kaklamanos *et al.* 2013). Other statistics relative to the considered parametrizations are reported by Paolucci *et al.* (2023).

All the considered *Vs* profiles are provided as Supporting Information.

## 3 SIMULATING HVSR CURVES

Simulations of the HVSR curves relative to the seismo-stratigraphical profiles described above have been performed by using computational tools described in the literature and provided in the form of freeware codes by the proponents. The code 'ModelHVSR' by Herak (2008) has been used to compute the HVSR curve under the assumption that it is determined by the vertically propagating body waves (acronym BW standing for 'Body Waves'). HVSR from ellipticity of the fundamental mode of Rayleigh waves (acronym R0 standing for Rayleigh Waves in the fundamental mode) in the far field by not considering sources were computed within the GEOPSY environment (Wathelet *et al.* 2020). HVSR resulting from the hypothesis that ambient vibrations result from the contribution of uncorrelated random point sources uniformly distributed at the Earth surface under the assumption that surface waves (Rayleigh and Love phases both in their fundamental and higher modes of propagation) dominate the wavefield has been deduced by the implementation of the formulas described by Lunedei & Albarello (2009); in this computational model, the respective importance of Rayleigh and Love phases is not fixed in advance but determined by the interplay between orientation of the random sources (here assumed to have the same average amplitude in the three Cartesian directions) and subsoil configuration. In the same model, the possibility is offered to consider only the contribution of Rayleigh waves in the fundamental mode (acronym 'DSS R0', standing for 'Distributed Surface Sources—Rayleigh waves in the fundamental mode') or to include Rayleigh and Love phases with the respective higher modes (acronym 'DSS SW' standing for 'Distributed Surface Sources—Surface Waves'). The code implementing the extension of this model to the full wavefield condition by considering correlated surface sources (Lunedei & Albarello 2015) has also been used (acronym 'DSS FW', standing for 'Distributed Surface Sources—Full Wavefield'). To compute HVSR assuming the diffuse character of ambient vibration wavefield propagating within an elastic layered subsoil, numerical code 'HVInv' (Garcia-Jerez *et al.* 2016) has been used by considering the contribution of surface waves (Rayleigh and Love) in the fundamental mode (acronym 'DFA RL', standing for 'Diffuse Field Approach—Rayleigh and Love'), including higher modes (acronym 'DFA SW', standing for 'Diffuse Field Approach—Surface Waves') and those considering the full wavefield (acronym 'DFA FW', standing for 'Diffuse Field Approach—Full Wavefield'). Table 1 reports the whole suite of simulators along with the acronyms considered in the following. It is worth to note that, except in the case of the DFA RL, DFA SW and DFA FW subsoil is assumed as viscoelastic and the effect of linear damping is accounted for. In the case of the implementation of DFA models here considered, subsoil is assumed to be purely elastic.

In all the cases, the implementations of the numerical models originally provided by the respective authors have been used for numerical computations. All the numerical tools considered for computations are provided in the Supporting Information.

## 4 STATISTICAL ANALYSIS

Some examples of HVSR curves determined by using the numerical tools listed in Table 1 are reported in Fig. 1. Despite the amplitude differences, the general similarity among the shape of HVSR curves appears evident, at least in a broad sense. This first glance impression is corroborated by the statistical analysis of the outcomes obtained by considering the 1600 *Vs* profiles. Two features of the HVSR patterns of main interest for engineering and seismological applications, are considered for this purpose: the HVSR maxima (their frequencies and amplitudes) and the overall shape of the HVSR curve. HVSR maxima are generally associated with the presence of sharp impedance contrasts in the subsoil and represent the main outcome of extensive field surveys devoted to seismic microzonation studies (e.g. Caielli *et al*. 2020; Paolucci *et al*. 2021). In this regard, the relative HVSR maximum (with amplitude $A_0$) characterized by the lowest frequency $f_0$ (the fundamental soil resonance frequency) is of particular interest (see e.g. Zhu *et al.* 2020). Of main importance is also the overall shape of the HVSR curve which is considered for constraining the local *Vs* profile by the most advanced inversion procedures (e.g. Foti *et al.* 2011; Bignardi *et al.* 2016; Garcia-Jerez *et al.* 2016; Wathelet *et al.* 2020). Both the above features have been considered in comparing outcomes of the considered models in the range of potential geological and engineering interest (0.05–30 Hz). When no HVSR relative maximum exists in that range (i.e. the HVSR curve exhibits a monotonic or flat shape), the respective values of $f_0$, and $A_0$ are considered equal to zero. In most cases (more than 90 per cent) $A_0$ is also the absolute maximum of the HVSR curve which is in line with empirical observations (see e.g. Zhu *et al.* 2020).

To evaluate similarity of $f_0$ and $A_0$ values, the coefficient of variation (CV), that is the ratio between the standard deviation and the average of the values obtained by computational models in Table 1, has been considered: CV values well below 1, indicate a strong concentration of the considered values around the average value. The distribution of 1600 CV values related to the considered *Vs* profiles are reported in Fig. 2. The distribution of CV values indicates that $f_0$ estimates provided by the different computational models are closely concentrated with CV values lower than 0.2 in 75 per cent of cases, indicating that all tested models provide similar estimate of characteristic soil resonance frequencies relative to shear waves. Considerably more variable appear estimates of $A_0$ with CV values which, anyway, remain lower than 1.0 in about 75 per cent of cases.

To gain a deeper insight about $A_0$ values obtained by the considered computational models, the respective frequency distributions are reported in Fig. 3. One can see that computational models considering the surface waves contribution only (DFA RL, DSS SW and DFA SW) provide more dispersed and generally higher $A_0$ values with respect to the ones provided by other models: significant number of $A_0$ values computed by only considering the contribution of surface waves (DFA SW, DFA RL, SDD SW, DFA R0, R0) are larger than 20 (red bars in Fig. 3). Except in the case that the measured ambient vibration times-series is preliminary filtered to isolate the contribution of Rayleigh waves (e.g. Fotouhimehr *et al.* 2021), such large values are quite uncommon.

Another alternative parametrization of observed differences between the $f_0$ and $A_0$ values provided by the computational models is obtained by considering the goodness-of-fit index $S$ proposed by Anderson (2004) and in the form

$$S\ (p_1, p_2) = \exp\left[-\left(\frac{p_1 - p_2}{\min(p_1, p_2)}\right)^2\right], \quad (1)$$

where $p_1$ and $p_2$ are the values to be compared: $S$ reaches a maximum value 1 when the agreement is perfect and rapidly tends to 0 when the difference increases (see also Olsen & Mayhew 2010; Graves & Pitarka 2015). Both the parameters $f_0$ and $A_0$ where considered and respective outcomes are reported in Table 2.

As one can see, median $S$ values relative to $f_0$ result almost coincident ($S > 0.8$) for all couples of computational models. As

**Table 1.** Numerical tools considered for the simulation of HVSR curves.

| Seismic phases considered in the simulation | Acronym | Hypothesis about HVSR origin | References |
|---|---|---|---|
| Full wavefield | DSS FW | Distributed Surface Sources (DSS)—Full Wavefield | Lunedei & Albarello (2015) |
| Full wavefield | DFA FW | Diffuse Field Approach (DFA)—Full Wavefield | Garcia-Jerez *et al.* (2016) |
| Rayleigh and Love waves (fundamental and higher modes) | DFA SW | Diffuse Field Approach (DFA)—Surface Waves | Garcia-Jerez *et al.* (2016) |
| Rayleigh and Love wave (fundamental modes) | DFA RL | Diffuse Field Approach (DFA)—Surface Waves | Garcia-Jerez *et al.* (2016) |
| Rayleigh and Love waves (fundamental and higher modes) | DSS SW | Distributed Surface Sources—Surface Waves | Lunedei & Albarello (2009) |
| Rayleigh waves (fundamental mode) | DFA R0 | Diffuse Field Approach (DFA)—Rayleigh waves | Garcia-Jerez *et al.* (2016) |
| Rayleigh wave (fundamental mode) | DSS R0 | Distributed Surface Sources (DSS)- Rayleigh waves | Lunedei & Albarello (2009) |
| Rayleigh waves (fundamental mode) | R0 | Ellipticity of Rayleigh waves in the far field | Wathelet *et al.* (2020) |
| Body waves (P and S waves) | BW | Vertically propagating Body Waves (BW) | Herak (2008) |

concerns $A_0$, however, quite different values are obtained ($S$ values close to 0 in most cases). Surprisingly, a good agreement exists between $A_0$ estimates provided by the less comprehensive computational model (BW) and the most comprehensive ones (DFA FW and DSS FW). This could be the effect of the major role played by body waves close to the *Vs* resonance frequency (Albarello & Lunedei 2011)

It could be of some interest evaluating to what extent discrepancies among the different estimates of $A_0$ may depend on the subsoil configurations. In Fig. 4 the distribution of CV values corresponding to $A_0$ estimates relative to considered subsoil configurations are reported. As expected, configurations of Class A (stiff soils) show general absence of peaks in the HVSR curves for all the models (CV = 0). Dispersion tends to increase as Vs30 values decrease passing from soils of Class B to soil of Class C.

As concerns the overall shape of the HVSR curves, similarities apparent in the examples in Fig. 1 are confirmed by a correlation analysis: median correlation values relative to each pair of computed HVSR curves are reported in Table 2. Pearson and Kendall rank correlation coefficients have been used and provide quite similar results.

Data in Table 3 confirm the impression obtained by examining Fig. 1 and indicate that HVSR curves for all 1600 seismostratigraphical configurations exhibit significant similarities, with median correlation values mostly above 0.7 both by considering Pearson and Kendall correlation coefficients. It is worth to note, that if the correlation is restricted to HVSR values below 10 Hz (i.e. to the range of main interest for engineering purposes), correlation values generally increase up to values 20 per cent. This suggests that most differences in the HVSR pattern occur in the high frequency range where numerical instabilities may play a major role (see Fig. 1 as an example).

Higher correlation values (well above 0.9) are found comparing outcomes relative to models accounting for the same seismic phases: full wavefield (DSS FW and DFA FW), surface waves (DSS SW, DFA SW and DFA RL), Rayleigh waves ellipticity (DFA R0, DSS R0 and R0). This finding suggests that background assumptions regarding the distribution of sources or the diffusive character of the ambient vibration wavefield are of minor importance in the definition of the HVSR curves. Much more important seems to be the role of seismic phases assumed to dominate the ambient vibration wavefield.

If one considers as reference the HVSR curves deduced under the most general conditions, that is considering all seismic phases (DSS FW and DFA FW), it is observed that the assumption of the wavefield dominated by surface waves (both Rayleigh and Love components) provides HVSR curves quite similar to the reference ones (correlation values above 0.85), while the assumption that only Rayleigh waves dominate appears less effective. What is quite surprising is the effectiveness of the simple body wave model BW which, despite its simplicity, provides HVSR curves very similar to the most general ones.

## 5 DISCUSSION AND CONCLUSION

In the pragmatistic view (e.g. Bernstein 2010), different models providing the same outcome are the same model (*'they state the same thing by using different words'*, Calderoni & Vailati 1931). In this line of reasoning, one should consider how much are the computational models in Tab. 1 actually different. In fact, all the models consider the propagation of small amplitude seismic waves within a viscoelastic linear medium constituted by a stack of uniform flat layers. This implies that the computation of spectral amplitudes ultimately rely on the same formalization based on the relevant Green's function or the equivalent propagator matrices (e.g. Kennett 2009). Moreover, since we are dealing with a stack of uniform layers, wave propagation can be represented in terms of upward and downward travelling waves, whose vertical and horizontal amplitudes depend on reflection/transmission matrices representative of boundary conditions at the layer interfaces. These matrices are independent of the sources responsible for the seismic perturbation, and their characteristics (and, in particular, their singularities) control main propagation effects in the layered medium concerning both surface and body waves. This may explain the fact that HVSR curves, however computed, show maxima at the same set of frequencies (Fig. 2). Main differences among the models in Table 1 only reflect which part of the Green's function is actually considered in computation, the possible role of source distribution, radiation

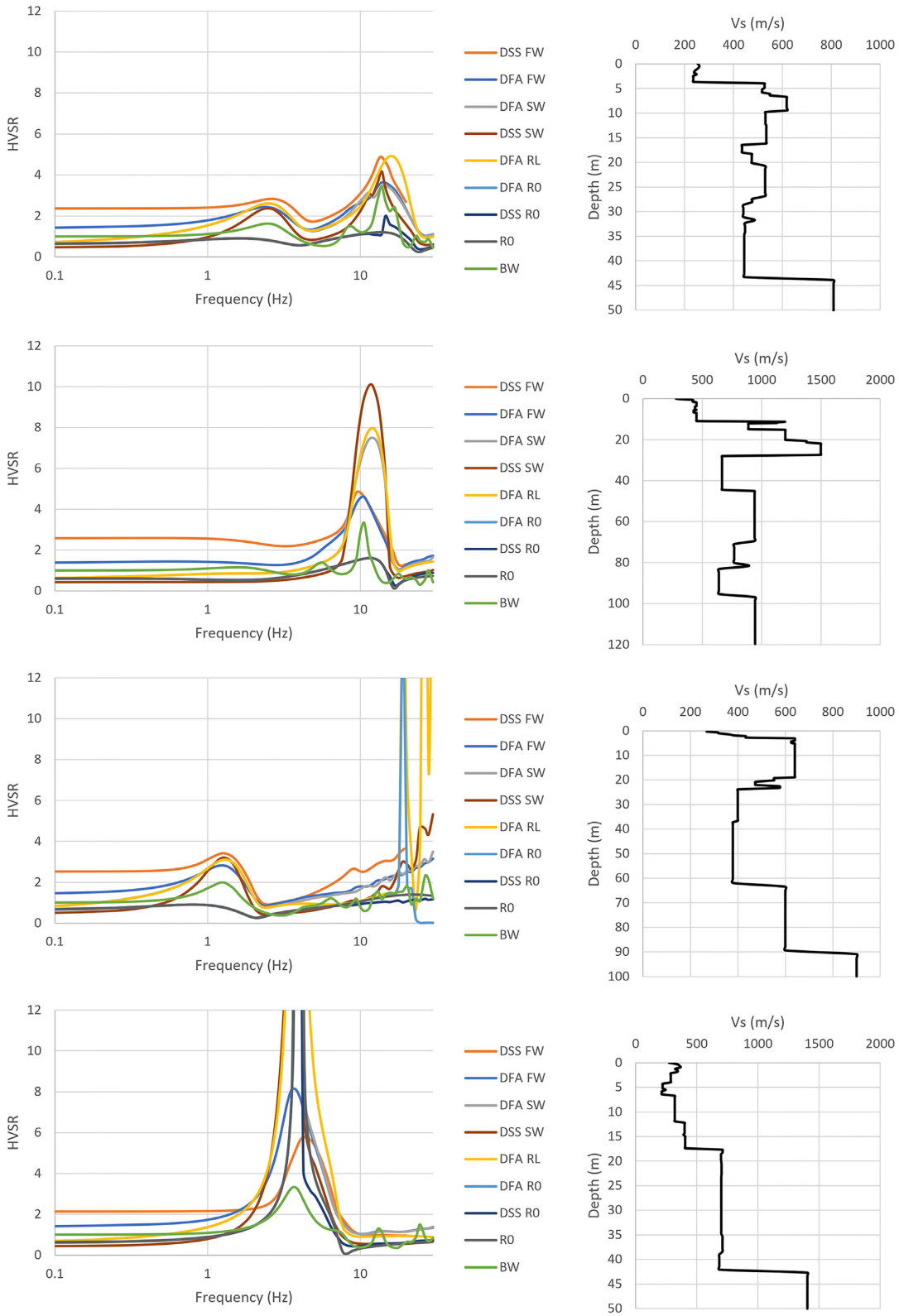


**Figure 1.** HVSR curves in the range 0.1–30 Hz simulated by the computational models in Table 1 relative to the four seismo-stratigraphical profiles (EC8 soil class B) shown to the right of the respective HVSR curves.

effects or scattering. The fact that the most comprehensive models (DFA FW and DSS FW) and the simplest one (BW) provide very similar HVSR curves suggests that these last aspects may play a minor role in the simulation of the HVSR curve.

On the other hand, correlation values indicate that HVSR curves computed by the different models are quite similar but not identical (See Fig. 1) and these differences mainly concern the overall amplitudes of the HVSR values (see Table 2 and Fig. 3). HVSR

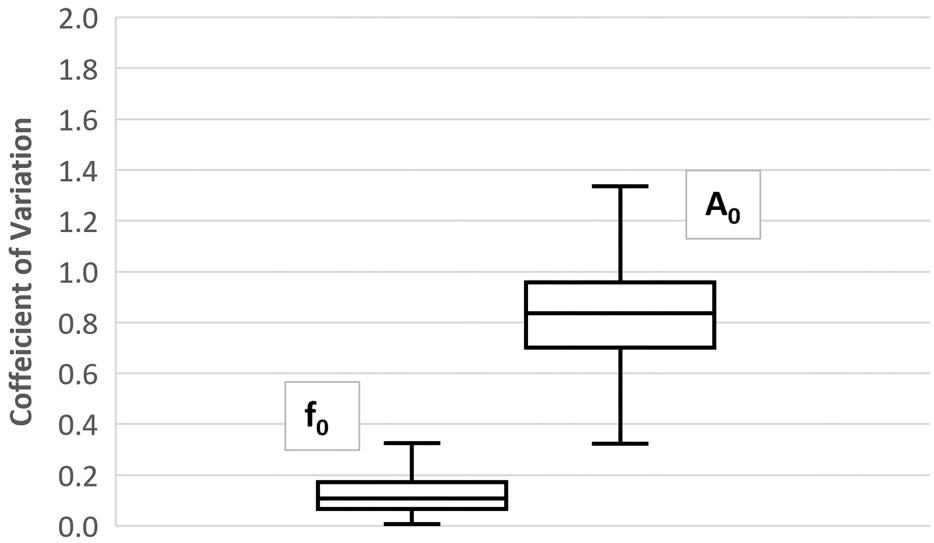


**Figure 2.** Box–Whiskers representation of the frequency distributions of the values of the coefficient of variation (CV) related to $A_0$ and $f_0$ values obtained by numerical simulations. Each box bounds the first and third quartile of the data distribution; the median is indicated by the horizontal line within the box. The vertical whiskers extend to 1.5 times the respective quartile and aim at covering the tails of the distribution.

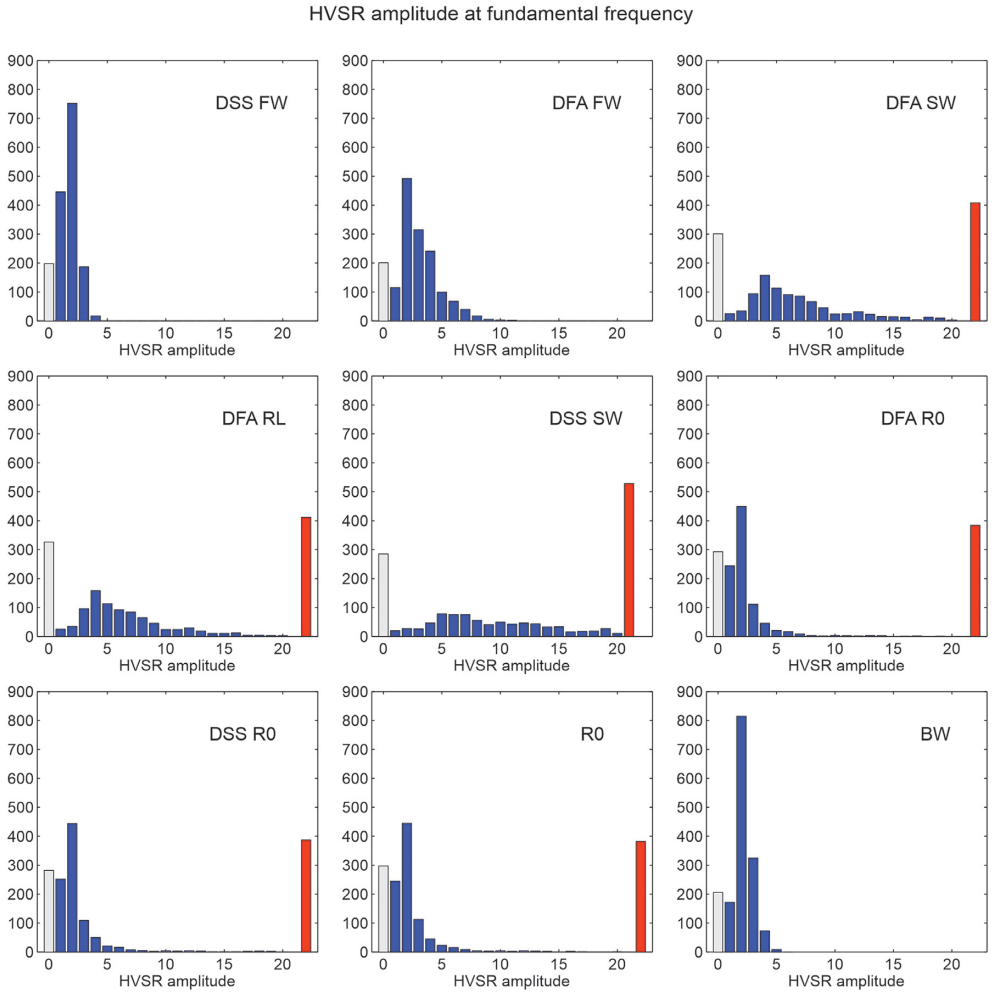


**Figure 3.** Histograms of the distribution of $A_0$ for the nine models. The rightmost bar (red) shows frequencies for all $A_0 > 20$ merged together; the leftmost bar (light grey) represents the cases identified as bedrock (with no maxima in the considered frequency range).

**Table 2.** Medians of the goodness-of-fit parameter $S$ by Anderson (2004) for the fundamental resonance frequency $f_0$ and the respective HVSR amplitude $A_0$ computed for the 1600 seismo-stratigraphical profiles by using the considered numerical models in the frequency range 0.05–30 Hz. Misfit values relative to $f_0$ and $A_0$ are, respectively, reported in the upper and lower triangular part of the matrix.

| $f_0/A_0$ | DSS FW | DFA FW | DSS SW | DFA SW | DFA RL | DFA R0 | DSS R0 | R0 | BW |
|---|---|---|---|---|---|---|---|---|---|
| DSS FW | | 0.97 | 0.96 | 0.96 | 0.95 | 0.80 | 0.81 | 0.81 | 0.97 |
| DFA FW | 0.51 | | 0.96 | 0.96 | 0.95 | 0.82 | 0.83 | 0.82 | 1.00 |
| DSS SW | 0.00 | 0.00 | | 1.00 | 1.00 | 0.92 | 0.94 | 0.92 | 0.95 |
| DFA SW | 0.00 | 0.00 | 0.00 | | 1.00 | 0.93 | 0.93 | 0.93 | 0.95 |
| DFA RL | 0.00 | 0.00 | 0.00 | 1.00 | | 0.97 | 0.96 | 0.97 | 0.96 |
| DFA R0 | 0.51 | 0.86 | 0.00 | 0.00 | 0.00 | | 1.00 | 1.00 | 0.80 |
| DSS R0 | 0.51 | 0.80 | 0.94 | 0.00 | 0.00 | 1.00 | | 1.00 | 0.80 |
| R0 | 0.50 | 0.85 | 0.00 | 0.00 | 0.00 | 1.00 | 1.00 | | 0.81 |
| BW | 0.92 | 0.80 | 0.00 | 0.00 | 0.00 | 0.77 | 0.73 | 0.42 | |

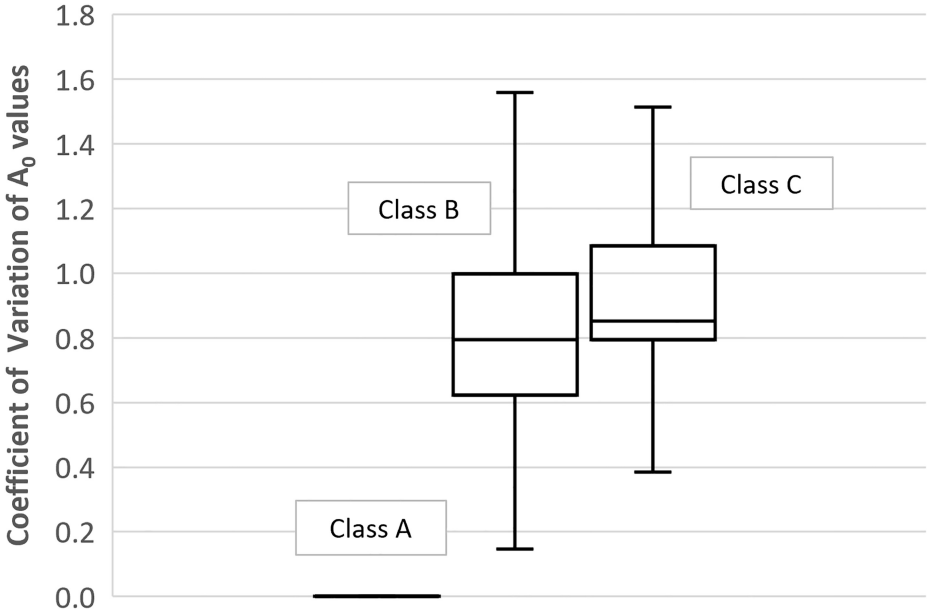


**Figure 4.** Box–Whiskers representation of the frequency distributions of the values of the coefficient of variation relative to the amplitude $A_0$ of the HVSR maxima obtained by the numerical simulations for soil classes A, B and C (see Fig. 2 for explanation).

**Table 3.** Medians of the correlation coefficients relative to HVSR curves computed for the 1600 seismo-stratigraphical profiles by using the considered numerical models in the frequency range 0.05–30 Hz. Pearson and Kendall correlation coefficients are, respectively, reported in the upper and lower triangular part of the matrix.

| | DSS FW | DFA FW | DSS SW | DFA SW | DFA RL | DFA R0 | DSS R0 | R0 | BW |
|---|---|---|---|---|---|---|---|---|---|
| DSS FW | | 0.95 | 0.83 | 0.82 | 0.77 | 0.72 | 0.74 | 0.73 | 0.82 |
| DFA FW | 0.84 | | 0.90 | 0.94 | 0.86 | 0.77 | 0.77 | 0.78 | 0.87 |
| DSS SW | 0.76 | 0.81 | | 0.99 | 0.89 | 0.73 | 0.75 | 0.73 | 0.73 |
| DFA SW | 0.73 | 0.85 | 0.93 | | 0.95 | 0.79 | 0.78 | 0.79 | 0.72 |
| DFA RL | 0.74 | 0.80 | 0.86 | 0.87 | | 0.93 | 0.88 | 0.91 | 0.64 |
| DFA R0 | 0.75 | 0.74 | 0.62 | 0.64 | 0.63 | | 1.00 | 1.00 | 0.62 |
| DSS R0 | 0.75 | 0.74 | 0.62 | 0.64 | 0.63 | 0.99 | | 1.00 | 0.62 |
| R0 | 0.75 | 0.74 | 0.62 | 0.64 | 0.63 | 0.99 | 0.99 | | 0.62 |
| BW | 0.68 | 0.68 | 0.60 | 0.60 | 0.57 | 0.61 | 0.61 | 0.61 | |

amplitudes depend on several factors (convention adopted to combine horizontal components, discarding or including surface waves higher modes, parametrization of material damping, etc.) and each model possibly shows different sensitivity to each of the soil parameters (damping, Poisson ratio, seismic impedance, distribution and character of sources, etc.) and subsoil *Vs* layering (see Fig. 4). Thus, in principle, an 'optimal' computational model could be useful to gain information about these parameters. However, such optimality cannot be assessed on theoretical basis. All the considered models only represent more or less comprehensive approximations of the underlying physical process, each justified by computational considerations. First, considering Earth as a stack of uniform viscoelastic layers contradicts seismological, geological, and geotechnical evidence about the complex structure of the subsoil close to the surface: this approximation may be effective in quite specific situations and frequency intervals. Moreover, the assumption that the ambient

vibration wavefield is isotropic (at least in the horizontal plane) does not account for the possible azimuthal variations in the field sources (e.g. along the coastline when sea waves are mainly responsible of observed vibrations). Furthermore, energization of the wavefield in the vertical and horizontal directions may vary case by case due to the relevant physical phenomenon (sea waves interference, barometric variations, wind, etc.) and this is not accounted for by any of the models in Table 1. One should be aware that also the more inclusive models only capture part of the processes controlling the ambient vibration wavefield: while DFA FW model enhances the role of wave scattering (responsible for the diffuse character of the wavefield) the DSS FW one puts in evidence the role of distributed surface sources. On the other hand, simpler models (e.g. R0) may be more effective when the HVSR to be reproduced have been obtained from ambient vibration time series filtered to isolate the contribution of specific seismic phases (e.g. Fotouhimehr *et al.* 2021)

Finally, one should be aware that generalizations make the numerical procedures increasingly complex, troublesome, and exposed to numerical instabilities. These problems become progressively more important when a huge number of forward simulations are required in the non-linear inversion of observed HVSR curves (e.g. Picozzi & Albarello 2007; García-Jerez *et al.* 2016).

The results of numerical simulations described above have been obtained by considering a huge amount of *Vs* profiles mostly representative of soil EC8 soil classes A, B, C and marginally E. This implies that, in principle, they could not be representative of all possible situations. It is worth noting, however, that available databases relative to observed *Vs* profile indicate that the above EC8 categories (mostly B) largely dominate in different geological contexts by covering a broad range of possible configurations. Another limitation of seismo-stratigraphical configurations considered here relies on the simplified assumptions concerning values of damping, Poisson's moduli and density. Basically, these have been considered as constant (damping and Poisson's modulus) or inferred from *Vs* in the case of density (via *Vp* values deduced from the assumed value of the Poisson's modulus). Other choices were possible (e.g. by inferring *Vp* from *Vs* by using empirical relationships by Brocher 2005). Moreover, depth of the considered profiles was limited (less than 200 m form the surface). However, since our work was focusing on the performances of the considered computational models when applied to a variety of cases, what seemed to be important was covering a wide range of 'realistic' configurations and we do not expect that considering different parametrization may significantly change our statistics.

Specific analyses should be carried on in the future to evaluate the impact of the computational models here considered when applied for inverting experimental HVSR curves. Beyond possible numerical troubles, interaction between inversion strategy and forward modelling may play a role in providing correct results. This implies that any comparison should be carried on by implementing the different forward models in the same inversion protocol, which is well beyond the aims of this study. Future work may possibly clarify this important aspect.

## ACKNOWLEDGMENTS

Many thanks are due to Sheri Molnar and Mathieu Perton, who kindly reviewed the manuscript providing encouraging comments and useful suggestions, which helped us to improve the manuscript.

## DATA AVAILABILITY

In the Supporting Information, all the *Vs* profiles considered in the numerical simulations are provided along with the numerical codes used on purpose.

## REFERENCES

Albarello, D. & Lunedei, E., 2011. Structure of ambient vibration wavefield in the frequency range of engineering interest ([0.5,20] Hz): insights from numerical modelling, *Near Surf. Geophys.,* **9,** 543–559.

Amanti, M. *et al.*, 2020. Geological and geotechnical model definition for 3rd level seismic microzonation studies in Central Italy, *Bull. Earthq. Eng.,* **18,** 5441–5473.

Anderson, J. G., 2004. Quantitative estimate of the goodness of fit synthetic seismograms, in *Proceedings of the 13th World Conference on Earthquake Engineering,* B.B., Canada, August 1–6 2004, Paper n.243.

Arai, H. & Tokimatsu, K., 2004. *S*-wave velocity profiling by inversion of microtremor H/V spectrum, *Bull. seism. Soc. Am.,* **94**(1), 53–63.

Bard, P. - Y. *et al.*, 2005. Guidelines for the implementation of the H/V spectral ratio technique on ambient vibrations measurements, processing and interpretation, Deliverable D23.12 of the SESAME project, 62 pp, April 2005. Available at: http://www.SESAME-FP5.obs.ujf-grenoble.fr.

Bernstein, R. J., 2010. *The Pragmatic Turn,* John Wiley & Sons, ISBN: 978-0-745-64908-5, 300pp.

Bignardi, S., Mantovani, A. & Abu Zeid, N., 2016. OpenHVSR: imaging the subsurface 2D/3D elastic properties through multiple HVSR modeling and inversion, *Comput. Geosci.,* **93,** 103–113

Brocher, T. M., 2005. Empirical relations between elastic wave speeds and density in the Earth's crust, *Bull. seism. Soc. Am.,* **95,** 2081–2092.

Caielli, G. *et al.*, 2020. Extensive surface geophysical prospecting for seismic microzonation, *Bull. Earthq. Eng.,* **18,** 5475–5502.

Calderoni, M. & Vailati, G., 1931. *Il Pragmatismo,* Rocco Carabba, 239pp.

EN 1998-1, 2004. Eurocode 8: Design of structures for earthquake resistance – Part 1: General rules, seismic actions and rules for buildings [Authority: The European Union Per Regulation 305/2011, Directive 98/34/EC, Directive 2004/18/EC].

Ferrari, G., Albarello, D. & Martinelli, G., 2000. Tromometric measurements as a tool for crustal deformation interpretation, *Seismol. Res. Lett.,* **71**(5), 562–569

Finetti, I. R., 2005. *CROP Project: Deep Seismic Exploration of the Central Mediterranean and Italy*. Elsevier. eBook ISBN: 9780080457604

Foti, S., Parolai, S., Albarello, D. & Picozzi, M., 2011, Application of Surface wave methods for seismic site characterization, *Surv. Geophys.,* **32**(6), 777–825.

Foti, S., Lai, C. G., Rix, G. & Strobbia, C., 2015. *Surface Wave Methods for Near-Surface Site Characterization,* CRC Press, ISBN 9781138077737.

Fotouhimehr, M., Shabani, E., Cornou, C. & Azmi, P., 2021. Ambient noise wavefield decomposition and shear-wave velocity retrieval in the south of Tehran, Iran and in the Colfiorito basin, Italy, *J. appl. Geophys.,* **184,**.

García-Jerez, A., Piña-Flores, J., Sánchez-Sesma, F. J., Luzón, F. & Perton, M.,2016. A computer code for forward calculation and inversion of the H/V spectral ratio under the diffuse field assumption, *Comput. Geosci.,* **97,** 67–78.

Graves, R. & Pitarka, A., 2015. Refinements to the Graves and Pitarka (2010) broadband ground-motion simulation method, *Seismol. Res. Lett.,* **86**(1), 75–80.

Herak, M., 2008. ModelHVSR—a Matlab® tool to model horizontal-to-vertical spectral ratio of ambient noise, *Comput. Geosci.,* **34**(11), 1514–1526

Kaklamanos, J., Bradley, B. A., Thompson, E. M. & Baise, L. G., 2013. Critical parameters affecting bias and variability in site-response analyses using KiK-net downhole array data, *Bull. seism. Soc. Am,* **103,** 1733–1749.

Kennett, B., 2009. *Seismic Wave Propagation in Stratified Media,* ANU Press, doi:10.26530/OAPEN_459524, 288pp.

Kottke, A. & Rathje, E., 2008. Technical manual for Strata, Report No.: 2008/10. Pacific Earthquake Engineering Research Center, University of California, Berkeley.

Lanchet, C. & Bard, P. Y., 1994. Numerical and theoretical investigations on the possibilities and limitations of the Nakamura's technique, *J. Phys. Earth.,* **42,** 377–397

Lanchet, C. & Bard, P. Y., 1995. Theoretical investigations on the Nakamura's technique, in *Proceedings of the 3rd International Conference on Recent Advanced in Geotechnical Earthquake Engineering and Soil Dynamics, 2–7 April 1995, St. Louis (Missouri),* Vol. **II**.

Lunedei, E. & Albarello, D., 2009. On the seismic noise wave field in a weakly dissipative layered Earth, *Geophys. J. Int.,* **177**(3), 1001–1014.

Lunedei, E. & Albarello, D., 2010. Theoretical HVSR curves from full wavefield modelling of ambient vibrations in a weakly dissipative layered Earth, *Geophys. J. Int.,* **181,** 1093–1108. doi:10.1111/j.1365-246X.2010.04560.x (Erratum: *Geophys . J. Int*. 192:1342. doi:10.1093/gji/ggs047).

Lunedei, E. & Albarello, D., 2015. Horizontal-to-vertical spectral ratios from a full-wavefield model of ambient vibrations generated by a distribution of spatially correlated surface sources, *Geophys. J. Int.,* **201,** 1142–1155.

Lunedei, E. & Albarello, D., 2021. Synthetic spectral structure of the seismic ambient vibrations generated by a distribution of superficial random sources with a finite extension, *Soil Dyn Eartq. Eng.,* **151,** 106949.

Lunedei, E. & Malischewsky, P., 2015. A review and some new issues on the theory of the H/V technique for ambient vibrations, in *Perspectives on European Earthquake Engineering and Seismology,* Vol. 1: 34 Geotechnical, Geological and Earthquake Engineering, ed. Ansal, A., Springer, https://doi.org/10.1007/978-3-319-16964-4_15.

Malischewsky, P. G. & Scherbaum, F., 2004. Love's formula and H/V-ratio (ellipticity) of Rayleigh waves, *WAMOD9,* **40,** 57–67.

Marzorati, S. & Bindi, D., 2006. Ambient noise levels in north central Italy, *Geochem. Geophys.,* **7,** 9.

Molnar, S. *et al.*, 2022. A review of the microtremor horizontal-to-vertical spectral ratio (MHVSR) method, *J. Seismol.,* **26,** 653–685.

Moscatelli, M., Albarello, D., Scarascia Mugnozza, G. & Dolce, M., 2020. The Italian approach to seismic microzonation, *Bull. Earthq. Eng.,* **18,** 5425–5440.

Okada, H., 2003. *The Microseismic Survey Methods*, Geophysical Monograph Series n.12, Society of Exploration Geophysics, Tulsa, USA

Olsen, K. B. & Mayhew, J. E., 2010. Goodness-of-fit criteria for broadband synthetic seismograms, with application to the 2008 Mw5.4 Chino Hills, CA, Earthquake, *Seismol. Res. Lett.,* **81**(5), 715–723.

Paolucci, E., Albarello, D., D'Amico, S., Lunedei, E., Martelli, L., Mucciarelli, M. & Pileggi, D., 2015. A large scale ambient vibration survey in the area damaged by May-June 2012 seismic sequence in Emilia Romagna, Italy, *Bull. Earthq. Eng.,* **13**(11), 3187–3206.

Paolucci, E., Tanzini, A., Peruzzi, G., Albarello, D. & Tiberi, P., 2020. Empirical testing of a simplified approach for the estimation of 1D lithostratigraphical amplification factor, *Bull. Earthq. Eng,* **18,** 1285–1301.

Paolucci, E., Cavuoto, G., Cosentino, G., Coltella, M., Simionato, M., Cavinato, G. P. & Albarello, D., 2021. Large-scale seismic characterization of shallow subsoil of Northern Apulia (Southern Italy), *Geosciences,* **11,** 416.

Paolucci, E., Tanzini, A. & Albarello, D., 2023. From HVSR to site SH response function: potentiality and pitfalls inferred by 1D physical modelling, *Soil Dyn. Earthq. Eng.,* **165,** 107703.

Peruzzi, G., Albarello, D., Baglione, M., D'Intinosante, V., Fabbroni, P. & Pileggi, D., 2016. Assessing 1D seismic response in microzoning studies in Italy, *Bull. Earthq. Eng.,* **14,** 373–389.

Picozzi, M. & Albarello, D., 2007. Combining Genetic and Linearized algorithms for a two-step joint inversion of Rayleigh wave dispersion and H/V spectral ratio curves, *Geophys. J. Int.,* **169,** 189–200

Pieri, P., *et al.*, 2004. Plio-Pleistocene stratigraphic and tectonic evolution of the foreland-foredeep-chain system in Southern Italy, in *Field Trip Guide Book, P35,* Vol. **4,** pp. 1–44, APAT – Italian Agency for the Environmental Protection and Technical Services.

Sánchez-Sesma, F. J. *et al.*, 2011. A theory for microtremor H/V spectral ratio: application for a layered medium, *Geophys. J. Int.,* **186,** 221–225

Schwab, F. A. & Knopoff, L., 1972. Fast surface wave and free mode computations, in *Methods in Computational Physics,* pp. 87–180, ed. Bolt, B. A., Academic Press.

Toro, G. R., 1995. Probabilistic models of site velocity profiles for generic and site-specific ground-motion amplification studies, Technical Report 779574, Upton, New York, USA.

Wathelet, M., Chatelain, J. - L., Cornou, C., Di Giulio, G., Guillier, B., Ohrnberger, M. & Savvaidis, A., 2020. Geopsy: a user-friendly open-source tool set for ambient vibration processing, *Seismol. Res.Lett.,* **91**(3), 1878–1889.

Zhu, C., Cotton, F. & Pilz, M., 2019. Testing the depths to 1.0 and 2.5 km /s velocity isosurfaces in a velocity model for Japan and implications for ground-motion modeling, *Bull. seism. Soc. Am.,* **109,** 2710–2721.

Zhu, C., Cotton, F. & Pilz, M., 2020. Detecting site resonant frequency using HVSR: Fourier versus response spectrum and the first versus the highest peak frequency, *Bull. seism. Soc. Am.,* **110,** 427–440.

## SUPPORTING INFORMATION

Supplementary data are available at *GJI* online.

Albarello el al. Suppl. Mat.rar
Lunedei & Albarello (2009)

Please note: Oxford University Press is not responsible for the content or functionality of any supporting materials supplied by the authors. Any queries (other than missing material) should be directed to the corresponding author for the paper.